
This item was submitted to [Loughborough's Research Repository](#) by the author.
Items in Figshare are protected by copyright, with all rights reserved, unless otherwise indicated.

Viscoelastic characterisation of additively manufactured composites with nylon matrix: effects of type and orientation of fibres

PLEASE CITE THE PUBLISHED VERSION

<https://doi.org/10.1016/j.compositesb.2023.110815>

PUBLISHER

Elsevier

VERSION

VoR (Version of Record)

PUBLISHER STATEMENT

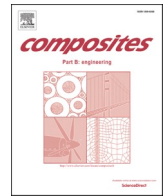
This is an Open Access Article. It is published by Elsevier under the Creative Commons Attribution-NonCommercial-NoDerivatives 4.0 International Licence (CC BY-NC-ND). Full details of this licence are available at: <https://creativecommons.org/licenses/by-nc-nd/4.0/>

LICENCE

CC BY-NC-ND 4.0

REPOSITORY RECORD

Islam, Md, Konstantinos Baxevanakis, and Vadim Silberschmidt. 2023. "Viscoelastic Characterisation of Additively Manufactured Composites with Nylon Matrix: Effects of Type and Orientation of Fibres". Loughborough University. <https://hdl.handle.net/2134/23283680.v1>.



Viscoelastic characterisation of additively manufactured composites with nylon matrix: Effects of type and orientation of fibres

Md Niamul Islam, Konstantinos P. Baxevanakis^{*}, Vadim V. Silberschmidt

Wolfson School of Mechanical, Electrical and Manufacturing Engineering, Loughborough University, LE11 3TU, UK

ARTICLE INFO

Handling Editor: Prof. Ole Thomsen

Keywords:

Additive manufacturing
Viscoelastic characterisation
Composite material
Dynamic mechanical analysis
Prony-series parameters

ABSTRACT

This study investigates the viscoelastic performance of additively manufactured (AM) nylon and nylon-matrix composites reinforced with short and continuous fibres with three different fibre orientations: longitudinal, transverse, and quasi-isotropic. Dynamic mechanical analysis under a frequency sweep of 1–100 Hz along with tensile tests used to determine the Young's modulus and X-ray micro-CT for evaluation of microstructural porosity were employed to fully describe the viscoelastic behaviour of the composites. Generally, the addition of fibres increased the storage modulus of most composites. The composites revealed increased porosity and fractography using a scanning electron microscope on the tensile specimens demonstrated poor fibre-matrix bonding. These factors, along with the fibre orientation, had a complex effect on the loss modulus of the composite structures. Overall, the addition of fibres reduced the damping factor of the composite specimens compared to pure AM nylon samples. The quantified parameters, including those of the Prony series, can be used in numerical simulations supporting the design and optimisation of AM components.

1. Introduction

The ability of additive manufacturing (AM) to produce complex geometrical structures with reduced material waste is its most valuable feature compared to traditional manufacturing processes. The technological advances and increased robustness of AM processes in the last decade have led to growing research in this field. The AM process can vary depending on the type (metal, polymer, ceramic) and phase (powder, filament, liquid) of the material [1,2]. Fused deposition modelling remains the most popular technique to produce AM structures from thermoplastic polymers such as polylactic acid (PLA), acrylonitrile butadiene styrene (ABS), and polyamides (nylon), where the raw material is extruded layer by layer through a heated nozzle. The solidification of the extruded filaments binds them to the adjacent layers, creating what is known as *material extruded additively manufactured* (MEAM) structures. The MEAM polymer structures have lower strength and stiffness compared to the bulk polymer due to microstructural defects such as voids/porosity [3–6]. These can be improved by optimising the manufacturing parameters such as layer height and print temperature but the best method to significantly enhance the performance of MEAM structures is by adding reinforcement materials, e.g., high-performance fibres (carbon fibre, glass fibre, Kevlar) to create

MEAM composite structures [7–9]. These fibres can be short (SFs), with the raw material for AM consisting of a mixture of a polymer matrix and SFs, extruded through a single nozzle [3,10–12], or they can be continuous (CFs), with the individual raw filaments of the nylon matrix and CFs extruded separately through different nozzles [4,10,11,13,14].

Generally, polymers exhibit both elastic and viscous behaviours known as *viscoelasticity* [15,16]; therefore, the stress in the polymer is related to the strain and strain rate due to the elastic and viscous nature, respectively. In the relaxation mode, the strain energy of the elastic component can be recovered but the viscous component causes permanent deformation, with the strain energy dissipated as heat in the process known as *viscous damping*. Therefore, investigation of the viscoelastic performance of polymer-matrix composites is essential for understanding the overall damping effect of these structures. Dynamic mechanical analysis (DMA) is a popular method to assess the viscoelastic performance of polymers and polymer-matrix composites at different temperatures and frequencies. Several studies analysed the viscoelastic characterisation of MEAM polymers and composites reinforced with SFs and CFs using DMA under temperature sweep as it allows the determination of their glass transition temperature [17–25]. However, very limited studies of DMA under frequency sweep can be found for such materials. The AM process and the addition of different types of fibre change the stiffness and microstructure of these polymers and

^{*} Corresponding author.

E-mail address: K.Baxevanakis@lboro.ac.uk (K.P. Baxevanakis).

Nomenclature

AM	Additive manufacturing
CF	Continuous fibres
CL	Nylon matrix reinforced with continuous carbon fibres in longitudinal orientation
CQ	Nylon matrix reinforced with continuous carbon fibres in quasi-isotropic orientation
CT	Nylon matrix reinforced with continuous carbon fibres in transverse orientation
IM	Injection moulded
MEAM	Material extruded additive manufacturing
N	AM nylon
NCCF	Nylon matrix reinforced with continuous carbon fibres
NSCF	Nylon matrix reinforced with short carbon fibres
SEM	Scanning electron microscopy
SF	Short fibres
SL	Nylon polymer matrix reinforced with short carbon fibres printed in longitudinal orientation
SQ	Nylon polymer matrix reinforced with short carbon fibres printed in quasi-isotropic orientation
ST	Nylon polymer matrix reinforced with short carbon fibres printed in transverse orientation

composites, and studies on traditional composites showed a link between stiffness and microstructure in the overall viscoelastic performance of these structures [26–29]. The addition of SFs and CFs in MEAM composites demonstrated a significant improvement of the stiffness of unidirectional MEAM composites loaded in the direction of fibres [3,4,10–12] but these fibres also increased the porosity with weaker bonding between fibre and matrix, thereby introducing new microstructural interfaces [3,4,10,13,30–32].

Current DMA research of MEAM polymers and composites lacks in-depth analysis of viscoelastic properties [33–35] in frequency sweep. This was also observed for traditional fibre-reinforced composites, especially, for the loss modulus with the general trends discussed but insufficient explanation of such phenomenon due to the absence of microstructural analysis [26–29]. This paper aims to fill this gap by thoroughly investigating the viscoelastic performance and microstructure of AM polymer/composites using DMA in a frequency-sweep regime. The influence of both short and continuous fibres (including their different orientations) on the stiffness and viscoelastic properties are explored, including its effect on the microstructure such as porosity to explain the overall damping factors of AM structures. Understanding

the viscoelastic properties of AM composites lays the foundation for an adequate analysis of their long-term performance as well as improving the design and optimisation of components for various applications.

2. Methodology

2.1. Materials and manufacturing methods

MEAM nylon and MEAM nylon-matrix composites reinforced with short and continuous carbon fibres, denoted NSCF and NCCF respectively, were investigated in the form of solid structures (100% infill) in this study. Nylon has good strength, stiffness and thermal resistance compared to other AM polymers such as PLA and ABS [36], while carbon fibre excels over other reinforcement fibres, for example, glass fibre and Kevlar in terms of strength and stiffness [37]. Raw filaments for NSCF were obtained from Polymaker (PA6-CF); they consist of nylon 6 with a 20% fibre volume fraction of chopped carbon fibres (length 250 μm), and the optical microscopy of the extruded filament confirmed it (Fig. 1a). The voids in the filament (red circle in Fig. 1) were found on its surface with scanning electron microscopy (SEM). CURA software and a Ultimaker 2+ printer were used to print the NSCF structures. For MEAM nylon and NCCF specimens, the raw materials were obtained from Markforged (white nylon and carbon-fibre spools), and the structures were fabricated using the Eiger software and Mark 2 printer. The NCCF structures were printed with a 20% volume fraction of continuous-fibre filament using Eiger but microscopy of the cross-section of this filament revealed 50–60% fibre (Fig. 1b), which ultimately reduced the effective fibre volume fraction in the NCCF structures to 10–12%. Table 1 summarises the printing parameters for MEAM nylon, NSCF and NCCF specimens.

Three different filament orientations – longitudinal, transverse, and quasi-isotropic – were considered for each type of fibre reinforcement. The NSCF and the NCCF filaments were extruded in the loading direction (0°) for the longitudinal orientation and perpendicular to this direction (90°) for the transverse orientation. For the complex quasi-isotropic structure, the filaments were printed at $0^\circ/+45^\circ/90^\circ/-45^\circ$ to reduce anisotropy introduced by the fibres in the MEAM composite structure. Table 2 lists the extruded-filament orientation of MEAM nylon

Table 1
Printing parameters of MEAM nylon polymer and composites.

Parameter	NCCF	NSCF	NSCF
Material	Nylon	Carbon fibre	Mixed
Nozzle temperature	260 $^\circ\text{C}$	260 $^\circ\text{C}$	260 $^\circ\text{C}$
Nozzle diameter	0.4 mm	0.9 mm	0.8 mm
Layer height	0.125 mm	0.125 mm	0.125 mm

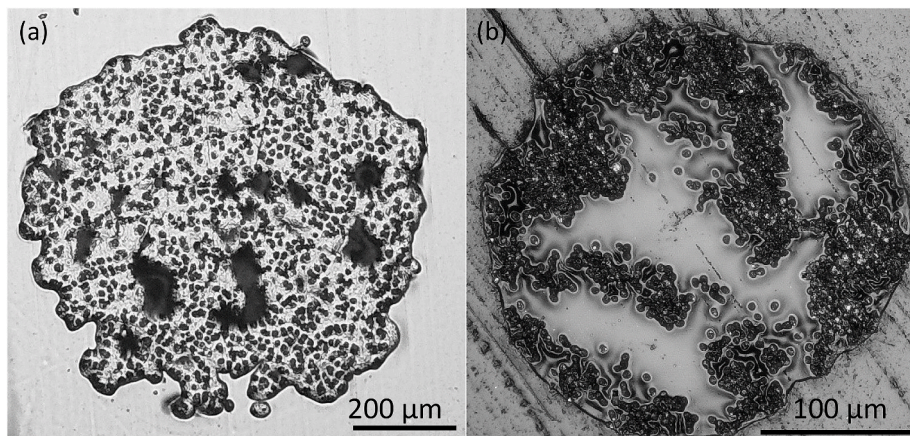
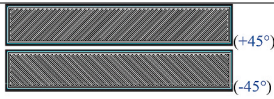





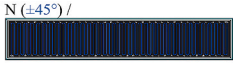


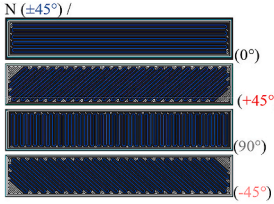

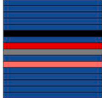






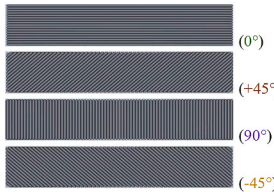
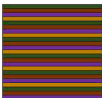
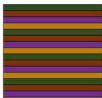
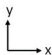
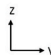
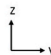


Fig. 1. Cross-section of NSCF filament (a) and NCCF fibre filament (b) under an optical microscope.

Table 2
Printing patterns and composite layups of MEAM nylon polymer and composites.

MEAM Structure	Matrix and/or fibre orientation	DMA – stack layup	Micro-CT/Tensile – stack layup
Pure nylon (N) ±45°	 (+45°) (-45°)		
		[±45°] ₂₄	[±45°] ₁₆
Pure nylon with 0° continuous fibre – longitudinal (CL)	 (0°)		
		[(±45°) ₄ /(+45°/0°/-45°/0°) ₂] ₆	[(±45°) ₄ /(+45°/0°/-45°/0°) ₅] ₆
Pure nylon with 90° continuous fibre – transverse (CT)	 (90°)		
		[(±45°) ₄ /(+45°/90°/-45°/90°) ₂] ₆	[(±45°) ₄ /(+45°/90°/-45°/90°) ₅] ₆
Pure nylon with 0°/45°/90°/-45° continuous fibre – quasi-isotropic (CQ)	 (0°) (+45°) (90°) (-45°)		
		[(±45°) ₄ /(+45°/0°/-45°/+45°/+45°/90°/-45°/-45°) ₅] ₆	[(±45°) ₄ /(0°/+45°/+45°/90°/-45°/-45°/-45°)/(±45°) ₅] ₆
Nylon + 0° short fibre – longitudinal (SL)	 (0°)		
		[0°] ₂₄	[0°] ₁₆
Nylon + 90° short fibre – transverse (ST)	 (90°)		
		[90°] ₂₄	[90°] ₁₆
Nylon + 0°/45°/90°/-45° short fibre – quasi-isotropic (SQ)	 (0°) (+45°) (90°) (-45°)		
		[0°/+45°/90°/-45°] ₆	[0°/+45°/90°/-45°] ₄
Coordinates			

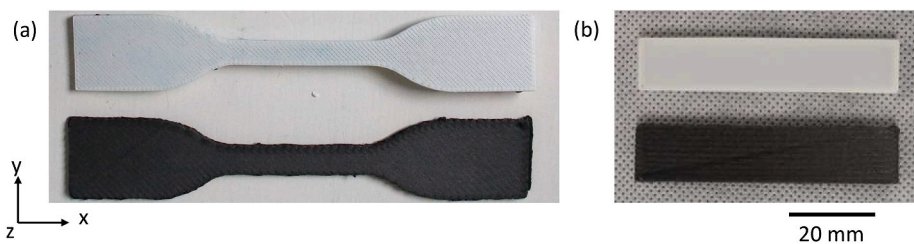


Fig. 2. MEAM NCCF (white) and NSCF (black) tensile (a) and DMA (b) specimens.

as well as of the MEAM NSCF and NCCF composite structures, including the stacking order for different mechanical tests.

2.2. Mechanical test and microstructural analysis

Tensile tests were carried out on 2 mm-thick specimens (Fig. 2a) according to the type IV specimen of ASTM D638 [38] at a speed of 5 mm min⁻¹ until fracture.

Dynamic mechanical analyses (DMA) were performed on 64 mm × 13 mm × 3 mm samples (Fig. 2b) following ASTM 5023 [39] in a 3-point bending configuration (Fig. 3) for a frequency sweep of 1–100 Hz at 5 Hz intervals at 22 °C. The 3-point bending setup was required for the process due to high stiffness of the fabricated AM nylon composite and thicker samples associated with the continuous-fibre laminated composite. The amplitude of the oscillations was 0.5 N; to ensure that the samples remained in contact with the vibrating shaft and the applied force was transferred to the sample throughout the complete oscillation, a preload force of 12 N was applied. There was no significant rise in the temperature of the samples during the whole frequency sweep process. The experiments were repeated at least 5 times for each case.

DMA applies a constant vibrating force, which leads to an oscillatory deformation over time of the samples. The cyclic strain on the sample due to this deformation along with the polymer’s viscoelastic nature demonstrates a lag between this applied strain and corresponding stress (Fig. 4) [15].

Therefore, the strain and the stress in the polymer in DMA can be described in the following form:

$$\epsilon = \epsilon_0 \sin \omega t, \tag{1}$$

$$\sigma = \sigma_0 \sin(\omega t + \delta), \tag{2}$$

where ϵ is the strain, ϵ_0 is the strain amplitude, σ is the stress, σ_0 is the stress amplitude, ω is the frequency, t is the time and δ is the phase lag [15,16]. The stress can then be decomposed into two components as follows

$$\sigma = \sigma_0 \cos \delta \sin \omega t + \sigma_0 \sin \delta \cos \omega t, \tag{3}$$

where the first magnitude $\sigma_0 \cos \delta$ is in phase with the strain and the second magnitude, $\sigma_0 \sin \delta$ is 90°, out of phase with strain.

These stresses can be related to storage modulus, G_s , and loss modulus, G_l :

$$G_s = \frac{\sigma_0}{\epsilon_0} \cos \delta, \tag{4}$$

$$G_l = \frac{\sigma_0}{\epsilon_0} \sin \delta. \tag{5}$$

The storage modulus is linked to the energy stored by the material through elastic deformation and the loss modulus to the energy lost to

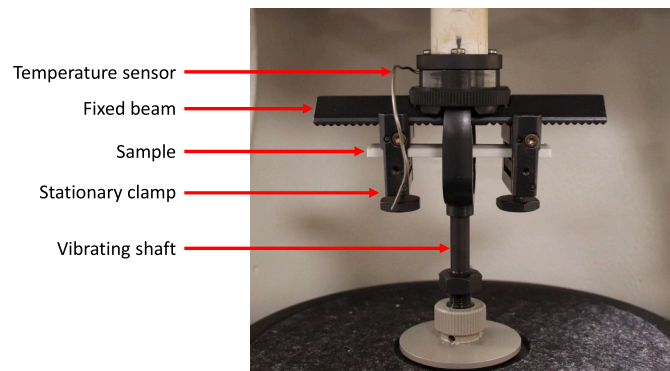


Fig. 3. 3-point bending configuration for DMA under frequency sweep.

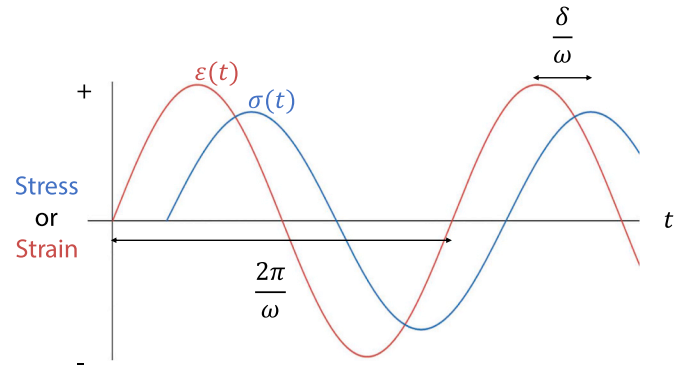


Fig. 4. Applied strain and corresponding stress response in polymer.

heat due to the viscous effect. Finally, the ratio between the loss and storage moduli is defined as the tan delta:

$$\tan \delta = \frac{G_s}{G_l}. \tag{6}$$

This quantity represents the energy lost to the energy stored by the material and measures its damping factor.

Micro-CT was performed on a 2 mm-thick specimen with a beam energy of 40 kV and beam current of 50 μA with 3016 projections to obtain high-resolution 3D images of the microstructure of the MEAM samples. The micro-CT results were post-processed using Dragonfly ORS software. Additionally, SEM was used on fractured surfaces post-tension to examine the structural bonding between the nylon matrix and the carbon fibres in AM composites.

3. Results and discussion

3.1. DMA of injection-moulded vs MEAM nylon polymer

The obtained levels of mean storage modulus, loss modulus, and tan delta for MEAM nylon specimens are summarised in Fig. 5 and the properties are compared against those of injection moulded (IM) nylon [28] for the DMA frequency sweep between 1 and 100 Hz in 3-point bending setup.

The storage modulus of MEAM nylon is initially lower than that of IM nylon, however, it increases with frequency, crossing the curve for IM nylon at 6 Hz. This significant increase in the storage modulus for MEAM nylon continues until 20 Hz, after which it rises gradually with

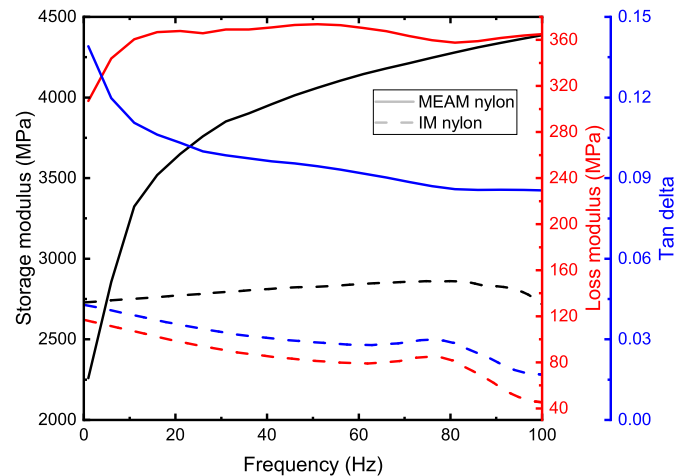


Fig. 5. Comparison of storage moduli, loss moduli and tan delta of nylon MEAM and IM specimens [28] for frequency sweep of 1–100 Hz.

frequency, whereas the increase in the storage modulus of IM nylon with frequency remains very small in comparison. This indicates that at raising frequency, MEAM nylon was able to store more energy through elastic deformation than IM nylon. However, a comparison for loss modulus showed that MEAM nylon had a significantly higher loss modulus compared to that of IM nylon for all corresponding frequencies, indicating that the former also lost more strain energy through viscous damping. However, the tan delta measures the ratio of energy lost to energy stored, which minimises the influence of external factors, and can be considered a structural property. The tan delta of MEAM nylon was significantly higher than that of IM nylon, indicating that the former has a higher contribution of viscosity, leading to higher dissipation of strain energy.

The MEAM process changes the microstructure of printed parts by introducing interfaces and voids between the extruded filaments. Fig. 6 shows the distribution of porosity in printed MEAM nylon structure (Supplementary Documents, Video 1 N). The friction at these interfaces during the shear deformation of the MEAM polymer and the compression of trapped air volumes in the pores led to higher strain-energy dissipation, increasing the damping effect. The decrease of the tan delta with frequency suggests that sufficient time was not provided for the polymers to disperse the energy at higher frequencies.

Guess [30] also showed a similar distribution of linear porosity for MEAM nylon with a significantly high level (36–39%) and concluded that poor fusion between the extruded filaments within the layers was its major source. However, in the current study, the porosity was lower (~10%), suggesting better bonding between the extruded filaments.

Supplementary video related to this article can be found at <http://doi.org/10.1016/j.compositesb.2023.110815>

3.2. Effect of fibres on Young's modulus and porosity

The measured values of the Young's modulus for MEAM nylon and the studied MEAM composites are shown in Fig. 7. The addition of fibres increased the stiffness similar to studies of MEAM nylon-matrix carbon-fibre-reinforced composites, where CFs had a significantly higher Young's modulus than SFs for longitudinal orientation [10,11,13]. However, for the transverse orientation, CFs had a lower Young's modulus compared to SFs. This is caused by the fact that the fibres are highly oriented and aligned perpendicular to the loading direction, with the nylon matrix carrying most of the load compared. The properties of the quasi-isotropic structure remained between those two cases, with CQ having higher stiffness than SQ thanks to more aligned fibres in the

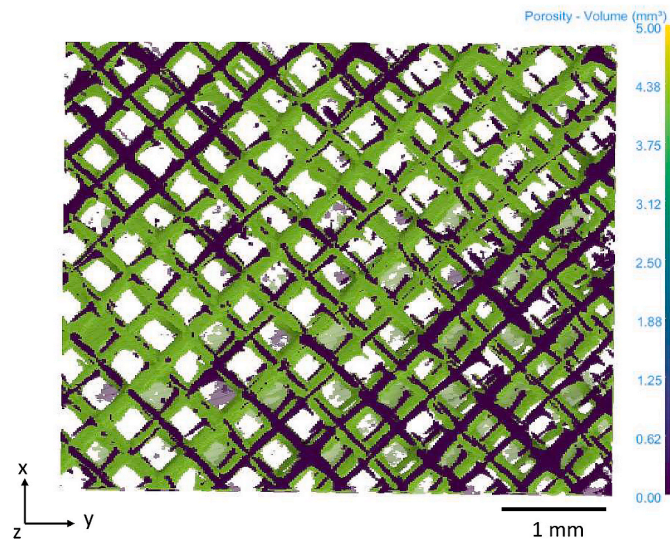


Fig. 6. Porosity distribution in MEAM nylon structure.

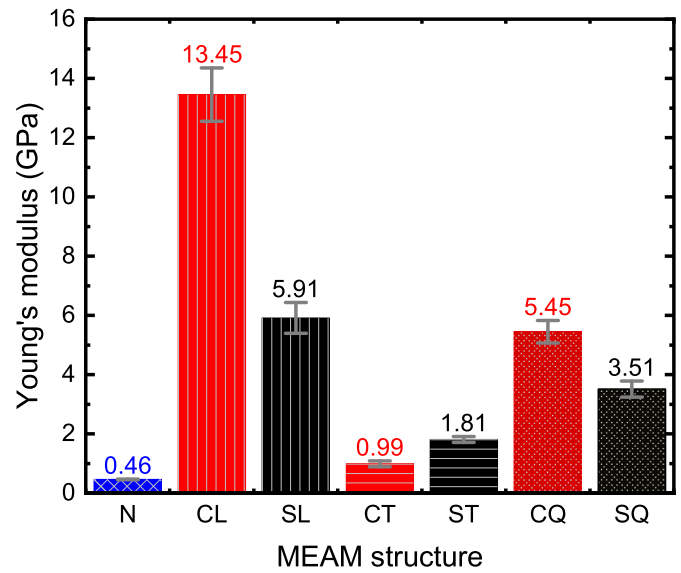


Fig. 7. Young's modulus of MEAM structures.

filaments.

The properties of the porosity in the MEAM structures are summarised in Table 3, with Fig. 8 demonstrating the distribution of microstructural porosity in them. The longitudinal and transverse specimens shared the same porosity properties as both were unidirectional structures with filaments rotated by 90° to the loading direction. The addition of fibres significantly increases the overall porosity of the MEAM structures due to the introduction of new fibre-matrix interfaces, while the type and orientation of these fibres also influenced the porosity. In general, the porosity of SF MEAM structures (Supplementary Documents, Video 2 SL and ST) was approximately 50% higher than that of the CF MEAM structures (Supplementary Documents, Video 3 CL and CT). For CFs, most of the porosity occurred between the separate layers of the composite, while for SFs the porosity was distributed throughout the whole structure. This indicates a poor bonding between fibres and the matrix since, for SF structures, the mixture of matrix-fibre extruded as a single filament created more interfaces, compared to the separate extrusion of the layered matrix and fibres in CF structures. On the contrary, the average pore volumes of CF structures were 50% larger than SF structures. This is expected as the SF structures are printed from a nylon-carbon fibre mixture in a single filament, which allowed the bonding of the nylon matrices between extruded filaments. However, in the CF structures, large pores were left between the separately extruded nylon and carbon-fibre layers.

Supplementary video related to this article can be found at <http://doi.org/10.1016/j.compositesb.2023.110815>

This pattern was also observed when comparing solid MEAM SF and CF composites, such as 16–27% for ABS with short carbon fibre [31] and 8.35% porosity for nylon with continuous carbon fibre [13]. Chisena et al. [32] showed 9.8% porosity for nylon with short carbon fibres; however, the analysis did not include pores between extruded filaments, leading to considerably lower porosity value compared to SF structure, but still higher compared to CF structures. The quasi-isotropic structure had slightly reduced porosity for both types of fibres, indicating that

Table 3
Porosity properties of MEAM structures.

Properties	N	CL/CT	SL/ST	CQ	SQ
Overall porosity (%)	10.08	13.98	20.08	11.05	18.77
Mean pore volume (mm ³)	0.0003	0.0003	0.0002	0.0003	0.0002
Average max Feret diameter (mm)	0.14	0.06	0.07	0.07	0.06

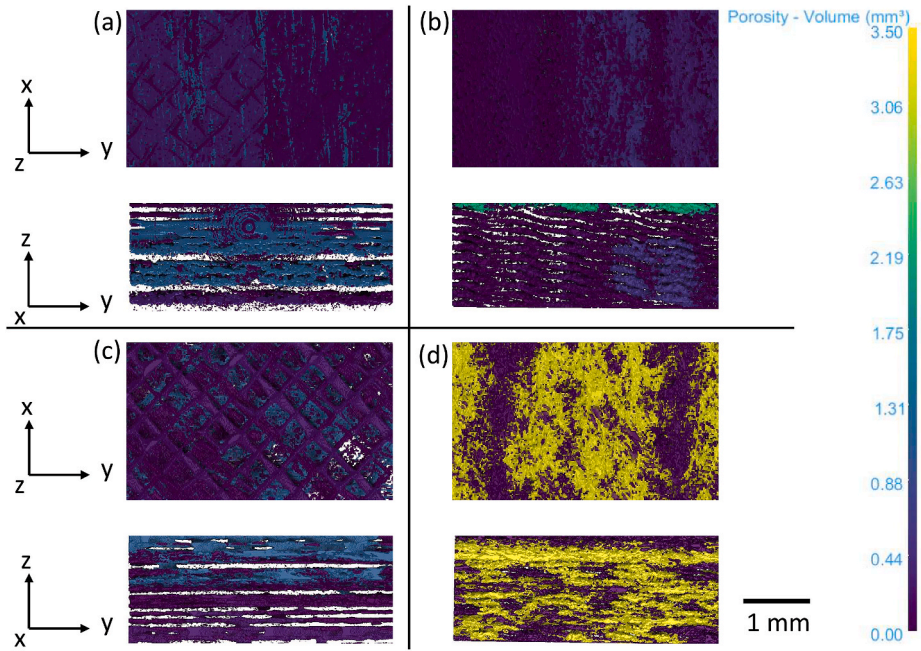


Fig. 8. Porosity distribution in MEAM composites: (a) CL/CT, (b) SL/ST, (c) CQ and (d) SQ.

changing the orientation across layers allows the extruded filaments to cross over each other and close some of the repeated gaps between the filaments (Supplementary Documents Video 4 SQ and Video 5 CQ). This was also observed in a similar study, where quasi-isotropic orientation almost halved the porosity compared to the unidirectional composite

[13].

Supplementary video related to this article can be found at <http://doi.org/10.1016/j.compositesb.2023.110815>

Further, the post-tensile fractography analysis of the MEAM structures (Fig. 9) revealed exposed fibres with surfaces, mostly clear of the

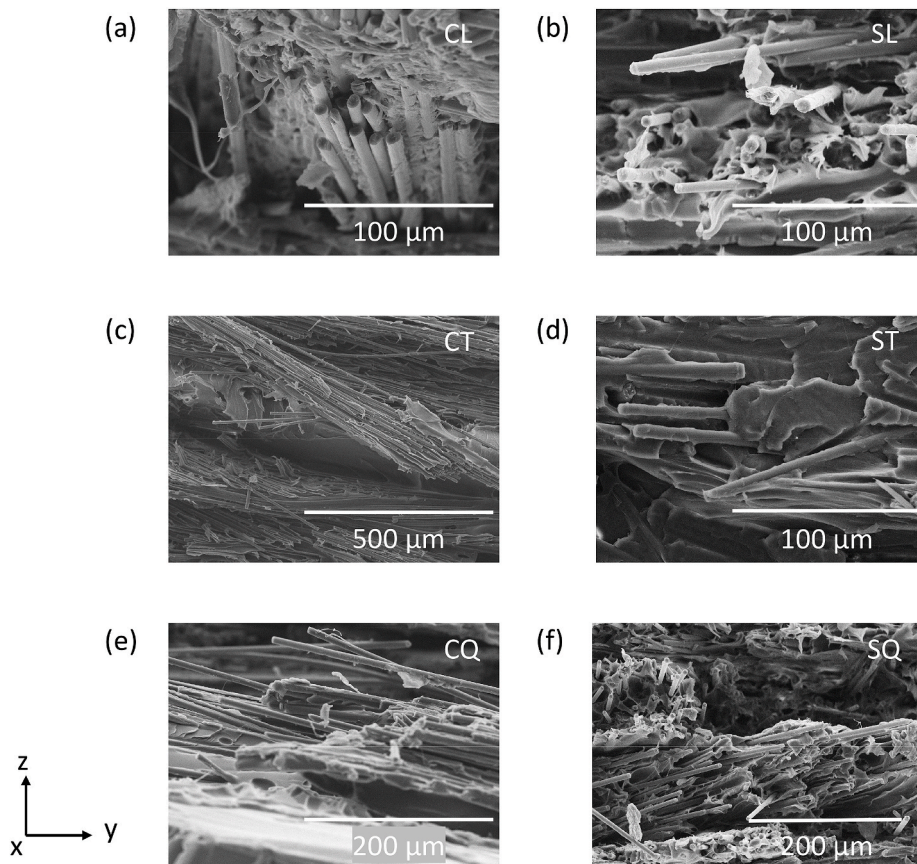


Fig. 9. SEM of fractured surfaces of MEAM tensile specimens.

matrix material, indicating poor bonding between the nylon matrix and carbon fibres. The SEM analysis of SF structures revealed no internal voids, in contrast to Fig. 1, confirming that they were only on the surface.

3.3. DMA of MEAM composites: storage moduli, loss moduli and tan delta

The mean storage modulus of the different MEAM structures from DMA with a 1–100 Hz frequency sweep at 22 °C are summarised in Fig. 10. The addition of fibres significantly increased the storage modulus of all the studied structures (see Fig. 5) (except for ST) thanks to their higher stiffness. For all MEAM structures, the storage modulus increased with frequency as the material was able to absorb more vibration energy introduced with increased frequency. The storage moduli of the CF structures were higher than that of the SF structures for the corresponding fibre orientation. Although ST had twice the Young's modulus of the MEAM nylon, the porosity was also twice as high and, therefore, there was less material in the structure to store the strain energy.

Similar studies of storage modulus of AM ABS material, nylon composites and stereolithographic graphene-polymer nanocomposites confirmed the link between storage modulus and Young's modulus [33–35]. This relation was also observed for polymer-matrix fibre-reinforced composites produced by other techniques such as oven baking [26], vacuum infiltration [27], and pre-peg layup [40].

The mean loss moduli of the MEAM structures obtained from DMA with a 1–100 Hz frequency sweep at 22 °C are shown in Fig. 11. The addition of fibres significantly increased the loss modulus of the MEAM structures except for ST, similar to the observation of the storage modulus response. The addition of fibres added fibre-matrix interfaces and increased the porosity within the MEAM structure. Slipping at these interfaces due to shear deformation caused friction, leading to higher dissipation of strain energy. Besides, the increased porosity led to the compression of more trapped air further increasing the viscous effects. However, unlike the storage modulus, the loss modulus of each structure fluctuated with increasing frequency, and the overall change was much lower. The loss modulus was influenced by the microstructural properties (porosity and fibre orientation), and the fluctuations occurred due to the microstructural uncertainties (small changes in porosities and fibre orientations due to deformation and vibration within the structures) at different frequencies.

Etaati et al. [26] demonstrated that for short hemp fibre, increasing the concentration increased the loss modulus of the structure up to 30% fibre volume and claimed that poor bonding of fibre-matrix caused the

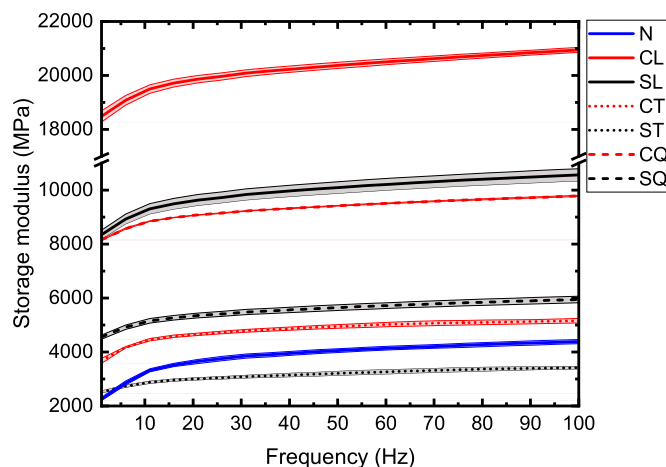


Fig. 10. Storage moduli of MEAM composite structures for frequency sweep of 1–100 Hz at 22 °C (shaded region based on error bars).

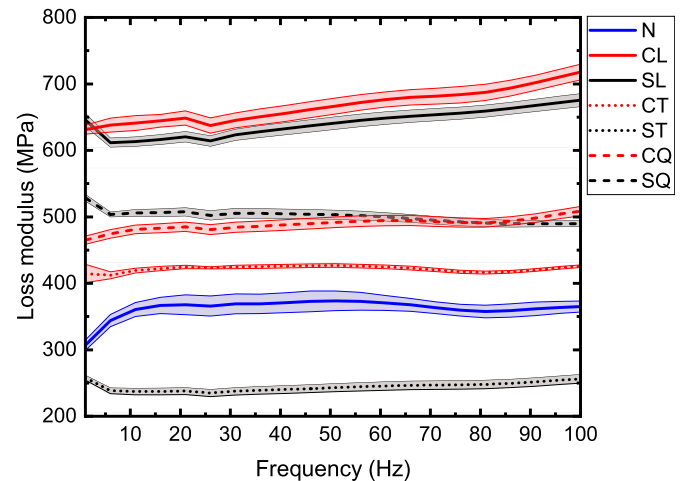


Fig. 11. Loss moduli of MEAM composite structures for frequency sweep of 1–100 Hz at 22 °C (shaded region based on error bars).

slipping and friction to dissipate the strain energy. Similarly, other studies found that the addition of nanofibres in the polymer increased the loss modulus of the structures [27,28]. However, most studies still lack an analysis of the reasons behind this phenomenon and point toward microstructural uncertainties.

Although there is a distinct effect of fibre orientation on the loss modulus, there is no clear relation between the type of fibres and their effect on the loss modulus. The longitudinal orientation had the highest loss modulus while the transverse one had the lowest; a similar observation was documented by Hadi [29], but there is still no satisfactory explanation for this phenomenon. The similarity of responses indicates that the orientation of the fibre-matrix interface plays an important role in energy dissipation. The mechanism of energy loss at the interface is shown in Fig. 12. Fibres pointing towards the direction of elastic wave (longitudinal orientation) have a higher extent of the interfacial surface along the direction of energy flow. As the energy propagates, the slipping of fibres at the fibre-matrix interfaces leads to more energy dissipation as heat, compared to fibres oriented perpendicular to the energy flow (transverse orientation). Since the quasi-isotropic orientation had a higher proportion of fibres in the direction of energy flow compared to the transverse orientation, the loss modulus was also higher. The fact that ST had a lower loss modulus than MEAM nylon was due to nylon having a significantly larger pore size and more oriented interfaces (linear porosity in the nylon matrix) in the direction of the strain energy compared to ST.

Next, the mean tan delta of the MEAM structures for a frequency sweep was analysed (Fig. 13). MEAM nylon had the highest tan delta for all frequencies, while the addition of fibres lowered the overall tan delta of the MEAM composites.

The tan delta of the structures reduced with the increase of frequency indicating lower energy was lost. The effect of type and orientation of fibres on the tan delta of the MEAM composites presented a complicated pattern due to the complexity in the response of loss modulus. Still, longitudinal is the most effective fibre orientation at reducing the damping factor of MEAM composites, with CFs remaining the best type of reinforcement to reduce the relative loss of strain energy (compared to the stored energy) by the MEAM composites unless the fibres are oriented in the transverse direction. Hence, CL demonstrated the lowest damping factor compared to the other MEAM composites. This observation matches with the study on MEAM nylon composites by Fernandes et al. [34], comparing the properties between short-fibre and short-fibre reinforced with continuous fibre structures, while our study investigated the effects of short and continuous fibre separately. The low tan delta of these structures indicates possible applications required to preserve the vibration energy of equipment, e.g., customised holders for electrical

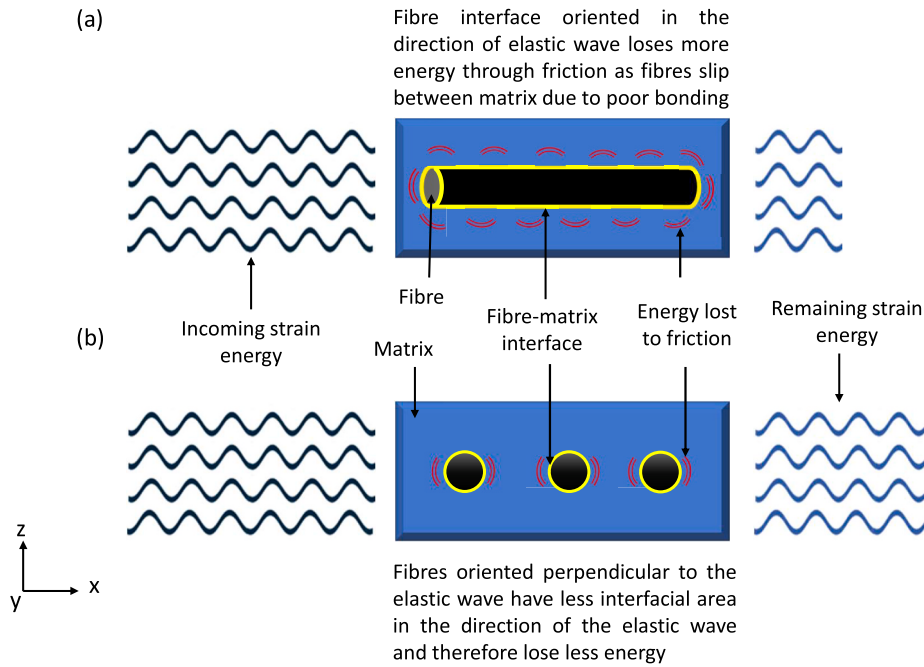


Fig. 12. Strain energy dissipation for fibres in longitudinal (a) and transverse (b) orientation.

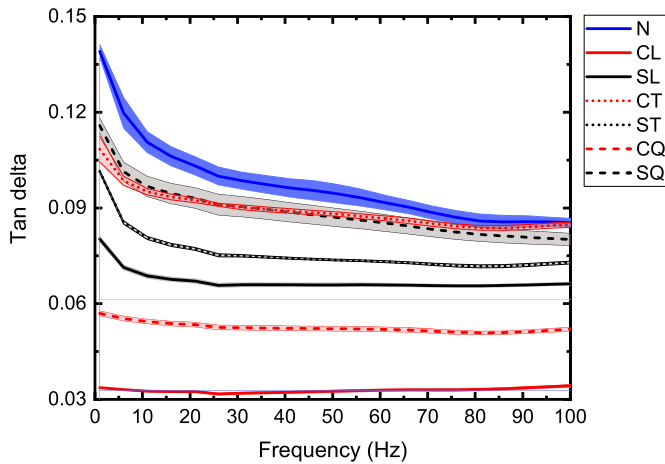


Fig. 13. Tan delta of MEAM composite structures for frequency sweep of 1–100 Hz at 22 °C (shaded region based on error bars).

drills and cutting instruments. The added stiffness and strength of fibre-reinforced structures with close levels of density for the nylon and carbon fibres provide the possibility to produce lightweight strong structures.

3.4. Calculating Prony-series parameters of MEAM structures

The Prony-series is used to describe the viscous behaviour of materials. In the time domain, it provides the dimensionless shear moduli as

$$G_R(t) = 1 - \sum_{i=1}^N G_i \left(1 - e^{-\frac{t}{\tau_i}}\right), \quad (7)$$

where G_R is the dimensionless shear modulus, t is time, and G_i, τ_i for $i = 1, 2, \dots, N$ are the material constants [41,42].

The Fourier transform is applied to Eq. (7) to present the storage and loss moduli in the frequency domain as

$$G_s(\omega) = G_0 \left(1 - \sum_{i=1}^N G_i\right) + G_0 \sum_{i=0}^N \frac{G_i \tau_i^2 \omega^2}{1 + \tau_i^2 \omega^2}, \quad (8)$$

$$G_r(\omega) = G_0 \sum_{i=0}^N \frac{G_i \tau_i \omega}{1 + \tau_i^2 \omega^2}, \quad (9)$$

where G_s and G_r are the storage and loss moduli, respectively, G_0 is the instantaneous shear modulus, and ω is the frequency.

The instantaneous shear modulus, G_0 was approximated as follows:

$$G_0 = \frac{E}{2(1 + \nu)}, \quad (10)$$

where E is the elastic modulus and ν is the Poisson's ratio estimated to be 0.25.

A generalised reduced gradient nonlinear solver was used to estimate the Prony-series parameters G_i and τ_i which were optimised for the corresponding number of terms N by minimising the squared residuals between the experimental values of the storage and loss moduli on the one hand, and G_s and G_r , on the other hand, calculated through the Prony series parameters, respectively.

The Prony-series parameters and the estimated magnitudes of the shear modulus for each MEAM structure are listed in Table 4. The experimental results and the Prony-series estimations for the storage and loss moduli with varying frequencies are compared in Fig. 14. The predictions with the Prony series matched well the experimental storage moduli thanks to their gradual increase with frequency for all the MEAM structures. However, the agreement was less perfect for the loss moduli case due to fluctuations of the experimental outputs with frequency; the mismatch was more pronounced where the changes were more abrupt (10–20 Hz). This is because the used algorithm prioritised the match of the storage modulus over the loss modulus as this reduced the total residual more (the sum of residuals of all frequencies) for the parameters. The process was repeated by incrementing N until the maximum residual was less than 2%, which was achieved for $N = 7$. The parameters obtained from the Prony-series calculation can be implemented in finite-element models to reproduce the viscoelastic response of the MEAM structures. This would introduce the damping effect for vibrating

Table 4
Prony-series parameters for MEAM composite structures.

MEAM structure	G_0	i	1	2	3	4	5	6	7
N	190	G_i	-25.6755	1.2861	3.5588	32.968	2.5861	2.4404	5.0326
		τ_i	0.000011	-0.011	0.0059	27.5293	-0.1413	0.0251	0.144
CL	5600	G_i	-4.9777	0.1493	2.1473	5.5026	0.0426	0.1409	0.2003
		τ_i	0.0004	-0.0061	0.0016	64.3977	-0.1364	0.0225	0.1493
SL	2460	G_i	-6.3323	0.058	3.1105	5.0063	0.0803	0.2832	0.4109
		τ_i	0.00085	-0.017	0.0024	24.2835	-0.1747	0.0252	0.1546
CT	410	G_i	-14.5433	0.3341	2.5442	22.8268	0.5319	1.3844	1.8378
		τ_i	-0.00042	-0.0105	-0.0001	27.8499	-0.2564	0.0219	0.1608
ST	750	G_i	-5.7866	0.3525	1.8866	6.8426	0.0963	0.5591	0.5383
		τ_i	-0.00057	-0.0101	-0.0005	24.4716	-0.2026	0.0172	0.143
CQ	2270	G_i	-5.168	0.1505	1.7839	7.4207	0.0525	0.2534	0.3394
		τ_i	0.00036	-0.007	0.0021	46.7627	-0.2054	0.0226	0.1505
SQ	1460	G_i	-4.6676	0.1319	1.563	2.636	0.0156	0.3463	0.477
		τ_i	0.00056	-0.0026	0.0034	9.0109	-0.7597	0.0249	0.1498

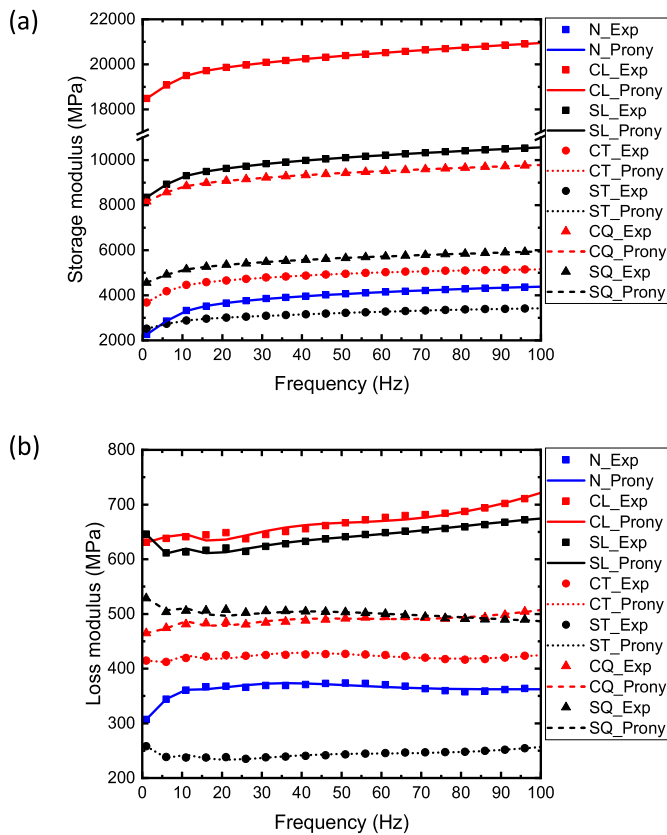


Fig. 14. Comparison of storage (a) and loss (b) moduli from DMA and their approximations with the Prony series.

structures and dynamic loading, providing a more adequate analysis of transient responses for various components.

4. Conclusions

The viscoelastic performance and microstructure of MEAM nylon and nylon matrix reinforced with short and continuous carbon fibre were investigated using DMA with a frequency sweep. Three different orientations of reinforcement fibres were analysed: longitudinal, transverse, and quasi-isotropic. The study revealed:

- MEAM nylon had a higher tan delta compared to IM nylon due to microstructural porosity introduced by the AM process. The friction at fibre-matrix interfaces and the compression of trapped air increased the dissipation of strain energy.

- The addition of fibres significantly increased the Young’s modulus of the MEAM composites. The longitudinal orientation had the highest Young’s modulus while the transverse was the lowest, with the quasi-isotropic one between them due to the orientation of fibres in the loading direction. CFs had a higher Young’s modulus than SFs for corresponding fibre orientation, except for ST, due to the continuous reinforcement within the structure. ST had a higher Young’s modulus than CT because some SFs were oriented in the loading direction.
- Fibres increased the porosity within the composite structures. The SFs resulted in higher porosity than the CFs due to an increased number of fibre-matrix interfaces. Also, the porosity in SFs was distributed throughout the whole structure whereas the porosity of the CFs was between the separate fibre-matrix layers. The quasi-isotropic orientation had lower porosity compared to that of the unidirectional structures due to crossings over the filaments. However, the pore size of SFs was 50% smaller than CFs.
- DMA revealed a direct relationship between the storage modulus and the Young’s modulus of the MEAM structures as the higher Young’s modulus allows more energy of elastic deformation to be stored. Also, an increase in the loss modulus with the addition of fibres was found due to increased porosity and fibre-matrix interfaces. The orientation of fibres played a major role as the longitudinal orientation lost more energy compared to the transverse one because more fibre-matrix interfaces were aligned along the direction of strain-energy propagation, and the slipping of fibres at interfaces led to higher energy losses caused by friction. The ST structure had a lower storage modulus due to higher porosity but a lower loss modulus due to smaller pores compared to the N structure.
- The overall tan delta values for MEAM composites were lower than that of MEAM nylon, with the longitudinal orientation (especially CL) having the lowest damping factor. Therefore, the addition of fibres and their influence on the microstructure can significantly affect the overall viscoelastic and damping properties of MEAM composites.
- Finally, the Prony-series parameters were obtained for the studied MEAM structures. The storage modulus fit well with the Prony parameters; however, there was some mismatch in the loss modulus at lower frequencies due to its fluctuation with frequency. Still, the overall error was below 2%; therefore, these parameters could be implemented for numerical modelling of the MEAM structures.

Author statement

Md Niamul Islam: Investigation, Data curation, Conceptualisation, Methodology, Formal analysis, Writing – original draft, Writing – review & editing, Visualisation.

Konstantinos P. Baxevanakis: Conceptualisation, Methodology, Formal analysis, Writing – review & editing, Supervision.

Vadim V. Silberschmidt: Conceptualisation, Methodology, Formal analysis, Writing – review & editing, Supervision.

Declaration of competing interest

The authors declare that they have no known competing financial interests or personal relationships that could have appeared to influence the work reported in this paper.

Data availability

Data will be made available on request.

References

- Arefin AME, Khatri NR, Kulkarni N, Egan PF. Polymer 3D printing review: materials, process, and design strategies for medical applications. *Polym (Basel)* 2021;13:1499. <https://doi.org/10.3390/polym13091499>.
- Ngo TD, Kashani A, Imbalzano G, Nguyen KTQ, Hui D. Additive manufacturing (3D printing): a review of materials, methods, applications and challenges. *Compos B Eng* 2018;143:172–96. <https://doi.org/10.1016/j.compositesb.2018.02.012>.
- Toro EV de, Sobrino JC, Martínez AM, Eguía VM, Pérez JA. Investigation of a short carbon fibre-reinforced polyamide and comparison of two manufacturing processes: fused Deposition Modelling (FDM) and polymer injection moulding (PIM). *Materials* 2020;13. <https://doi.org/10.3390/ma13030672>.
- Chacón JM, Caminero MA, Núñez PJ, García-Plaza E, García-Moreno I, Reverte JM. Additive manufacturing of continuous fibre reinforced thermoplastic composites using fused deposition modelling: effect of process parameters on mechanical properties. *Compos Sci Technol* 2019;181:107688. <https://doi.org/10.1016/j.compscitech.2019.107688>.
- Selva Priya M, Naresh K, Jayaganthan R, Velmurugan R. A comparative study between in-house 3D printed and injection molded ABS and PLA polymers for low-frequency applications. *Mater Res Express* 2019;6. <https://doi.org/10.1088/2053-1591/ab2776>.
- Carneiro OS, Silva AF, Gomes R. Fused deposition modeling with polypropylene. *Mater Des* 2015;83:768–76. <https://doi.org/10.1016/j.matdes.2015.06.053>.
- Wang X, Jiang M, Zhou Z, Gou J, Hui D. 3D printing of polymer matrix composites: a review and prospective. *Compos B Eng* 2017;110:442–58. <https://doi.org/10.1016/j.compositesb.2016.11.034>.
- Parandoush P, Lin D. A review on additive manufacturing of polymer-fiber composites. *Compos Struct* 2017;182:36–53. <https://doi.org/10.1016/j.compstruct.2017.08.088>.
- Krajangsawadi N, Blok LG, Hamerton I, Longana ML, Woods BKS, Ivanov DS. Fused deposition modelling of fibre reinforced polymer composites: a parametric review. *J Compos Sci* 2021;5. <https://doi.org/10.3390/jcs5010029>.
- Blok LG, Longana ML, Yu H, Woods BKS. An investigation into 3D printing of fibre reinforced thermoplastic composites. *Addit Manuf* 2018;22:176–86. <https://doi.org/10.1016/j.addma.2018.04.039>.
- Peng Y, Wu Y, Wang K, Gao G, Ahzi S. Synergistic reinforcement of polyamide-based composites by combination of short and continuous carbon fibers via fused filament fabrication. *Compos Struct* 2019;207:232–9. <https://doi.org/10.1016/j.compstruct.2018.09.014>.
- Hetrick DR, Sanei SHR, Bakis CE, Ashour O. Evaluating the effect of variable fiber content on mechanical properties of additively manufactured continuous carbon fiber composites. *J Reinforc Plast Compos* 2021;40:365–77. <https://doi.org/10.1177/0731684420963217>.
- Saeed K, McIlhagger A, Harkin-Jones E, McGarrigle C, Dixon D, Ali Shar M, et al. Characterization of continuous carbon fibre reinforced 3D printed polymer composites with varying fibre volume fractions. *Compos Struct* 2022;282. <https://doi.org/10.1016/j.compstruct.2021.115033>.
- Yu T, Zhang Z, Song S, Bai Y, Wu D. Tensile and flexural behaviors of additively manufactured continuous carbon fiber-reinforced polymer composites. *Compos Struct* 2019;225:111147. <https://doi.org/10.1016/j.compstruct.2019.111147>.
- Meyers MA, Chawla KK. *Mechanical behavior of materials*. second ed. Cambridge: Cambridge University Press; 2008. <https://doi.org/10.1017/CBO9780511810947>.
- Ward IM, Ian M, Sweeney J. *Mechanical properties of solid polymers*. third ed. 2012.
- Coppola B, Cappetti N, Maio L di, Scarfato P, Incarnato L. 3D printing of PLA/clay nanocomposites: influence of printing temperature on printed samples properties. *Materials* 2018;11. <https://doi.org/10.3390/ma11101947>.
- Billah KMM, Lorenzana FAR, Martínez NL, Wicker RB, Espalin D. Thermomechanical characterization of short carbon fiber and short glass fiber-reinforced ABS used in large format additive manufacturing. *Addit Manuf* 2020;35. <https://doi.org/10.1016/j.addma.2020.101299>.
- Seifans AM, Ayyagari S, Al-Haik M. Elastic/viscoplastic characterization of additively manufactured composite based on continuous carbon fibers. *Aero Sci Technol* 2021;111. <https://doi.org/10.1016/j.ast.2021.106562>.
- Pascual-González C, Iragi M, Fernández A, Fernández-Blázquez JP, Aretxabaleta L, Lopes CS. An approach to analyse the factors behind the micromechanical response of 3D-printed composites. *Compos B Eng* 2020;186. <https://doi.org/10.1016/j.compositesb.2020.107820>.
- Quiñonez PA, Ugarte-Sanchez L, Bermudez D, Chinolla P, Dueck R, Cavender-Word TJ, et al. Design of shape memory thermoplastic material systems for fdm-type additive manufacturing. *Materials* 2021;14. <https://doi.org/10.3390/ma14154254>.
- Jeyachandran P, Bontha S, Bodhak S, Balla VK, Doddamani M. Material extrusion additive manufacturing of bioactive glass/high density polyethylene composites. *Compos Sci Technol* 2021;213. <https://doi.org/10.1016/j.compscitech.2021.108966>.
- Mazurchevici SN, Mazurchevici AD, Nedelcu D. Dynamical mechanical and thermal analyses of biodegradable raw materials for additive manufacturing. *Materials* 2020;13. <https://doi.org/10.3390/MA13081819>.
- Raasch J, Ivey M, Aldrich D, Nobes DS, Ayranci C. Characterization of polyurethane shape memory polymer processed by material extrusion additive manufacturing. *Addit Manuf* 2015;8:132–41. <https://doi.org/10.1016/j.addma.2015.09.004>.
- Pu J, McIlroy C, Jones A, Ashcroft I. Understanding mechanical properties in fused filament fabrication of polyether ether ketone. *Addit Manuf* 2021;37. <https://doi.org/10.1016/j.addma.2020.101673>.
- Etaati A, Mehdiadeh SA, Wang H, Pather S. Vibration damping characteristics of short hemp fibre thermoplastic composites. *J Reinforc Plast Compos* 2014;33:330–41. <https://doi.org/10.1177/0731684413512228>.
- Jiang Z, Wang F, Yin J, Gong S, Dai Z, Pang Y, et al. Vibration damping mechanism of CuAlMn/polymer/carbon nanomaterials multi-scale composites. *Compos B Eng* 2020;199. <https://doi.org/10.1016/j.compositesb.2020.108266>.
- Xu X, Sanei SHR, Steinmetz E, Gohn A, Williams J. Effect of microstructure uncertainty and testing frequency on storage and loss moduli of injection molded MWCNT reinforced polyamide 66 nanocomposites. *Polym Test* 2020;85. <https://doi.org/10.1016/j.polymertesting.2020.106455>.
- Hadi AS, Ashton JN. Measurement and theoretical modelling of the damping properties of a uni-directional glass/epoxy composite. *Compos Struct* 1996;34:381–5. [https://doi.org/10.1016/0263-8223\(96\)00005-0](https://doi.org/10.1016/0263-8223(96)00005-0).
- Guessasma S, Belhabib S, Nouri H. Effect of printing temperature on microstructure, thermal behavior and tensile properties of 3D printed nylon using fused deposition modeling. *J Appl Polym Sci* 2021;138. <https://doi.org/10.1002/app.50162>.
- Tekinalp HL, Kunc V, Velez-Garcia GM, Duty CE, Love LJ, Naskar AK, et al. Highly oriented carbon fiber-polymer composites via additive manufacturing. *Compos Sci Technol* 2014;105:144–50. <https://doi.org/10.1016/j.compscitech.2014.10.009>.
- Chisena RS, Engstrom SM, Shih AJ. Computed tomography evaluation of the porosity and fiber orientation in a short carbon fiber material extrusion filament and part. *Addit Manuf* 2020;34. <https://doi.org/10.1016/j.addma.2020.101189>.
- Colón Quintana JL, Redmann A, Mazzei Capote GA, Pérez-Irizarry A, Bechara A, Osswald TA, et al. Viscoelastic properties of fused filament fabrication parts. *Addit Manuf* 2019;28:704–10. <https://doi.org/10.1016/j.addma.2019.06.003>.
- Fernandes RR, Tamijani AY, Al-Haik M. Mechanical characterization of additively manufactured fiber-reinforced composites. *Aero Sci Technol* 2021;113. <https://doi.org/10.1016/j.ast.2021.106653>.
- Lai CQ, Markandan K, Luo B, Lam YC, Chung WC, Chidambaram A. Viscoelastic and high strain rate response of anisotropic graphene-polymer nanocomposites fabricated with stereolithographic 3D printing. *Addit Manuf* 2021;37. <https://doi.org/10.1016/j.addma.2020.101721>.
- Lay M, Thajudin NLN, Hamid ZAA, Rusli A, Abdullah MK, Shuib RK. Comparison of physical and mechanical properties of PLA, ABS and nylon 6 fabricated using fused deposition modeling and injection molding. *Compos B Eng* 2019;176:107341. <https://doi.org/10.1016/j.compositesb.2019.107341>.
- Material Markforged. *Datashet - Composites* 2021;1–2.
- ASTM 638-14. Standard test method for tensile properties of plastics. *ASTM International* 2006:1–15. <https://doi.org/10.1520/D0638-14.1>.
- ASTM D5023-15. Standard test method for plastics: dynamic mechanical properties: in flexure (Three-Point bending). *ASTM International* 2007;9–12. <https://doi.org/10.1520/D5023-15.1>.
- Fouad H, Mourad AHL, Alshammari BA, Hassan MK, Abdallah MY, Hashem M. Fracture toughness, vibration modal analysis and viscoelastic behavior of Kevlar, glass, and carbon fiber/epoxy composites for dental-post applications. *J Mech Behav Biomed Mater* 2020;101. <https://doi.org/10.1016/j.jmbbm.2019.103456>.
- Jalocha D, Constantinescu A, Neviere R. Revisiting the identification of generalized Maxwell models from experimental results. *Int J Solid Struct* 2015;67(68):169–81. <https://doi.org/10.1016/j.ijsolstr.2015.04.018>.
- Smith M. *ABAQUS/Standard user's manual, version 6.9*. Dassault Systèmes Simulia Corp; 2009.